J Nanostruct Chem (2017) 7:345–358
https://doi.org/10.1007/s40097-017-0244-3

ORIGINAL RESEARCH

Molecular design of O_3 and NO_2 sensor devices based on a novel heterostructured N-doped TiO_2/ZnO nanocomposite: a van der Waals corrected DFT study

Amirali Abbasi[1,2,3] · **Jaber Jahanbin Sardroodi**[1,2,3]

Received: 31 August 2017 / Accepted: 26 October 2017 / Published online: 4 November 2017
© The Author(s) 2017. This article is an open access publication

Abstract We have presented a density functional theory study of the adsorption properties of NO_2 and O_3 molecules on heterostructured TiO_2/ZnO nanocomposites. The most stable adsorption configurations, adsorption energies and charge transfers were calculated. The electronic properties of the complex TiO_2/ZnO heterostructures were described using the density of states and molecular orbital analyses. For NO_2 adsorption, it was found that the oxygen atoms preferentially move towards the fivefold coordinated titanium atoms, whereas the nitrogen atom binds to the zinc atom. In the case of O_3 adsorption, the side oxygen atoms bind to the fivefold coordinated titanium sites, and the central oxygen atom does not contribute to the adsorption any longer. Thus, the interaction of NO_2 and O_3 molecules with TiO_2 side of nanocomposite is strongly favored. On the N-doped TiO_2/ZnO nanocomposites, the adsorption process is more energetically favorable than that on the pristine ones. The N-doped nanocomposites are far more sensitive to gas detection than the undoped ones. In TiO_2/ZnO nanocomposites, the interactions of gas molecule and TiO_2 are stronger than those between gas molecule and bare TiO_2 nanoparticles, which reveals that ZnO is conducive to the interaction of NO_2 and O_3 molecules with TiO_2 nanoparticles. Our theoretical results suggest multicomponent TiO_2/ZnO nanocomposite as a potential material for gas sensing application.

Graphical Abstract

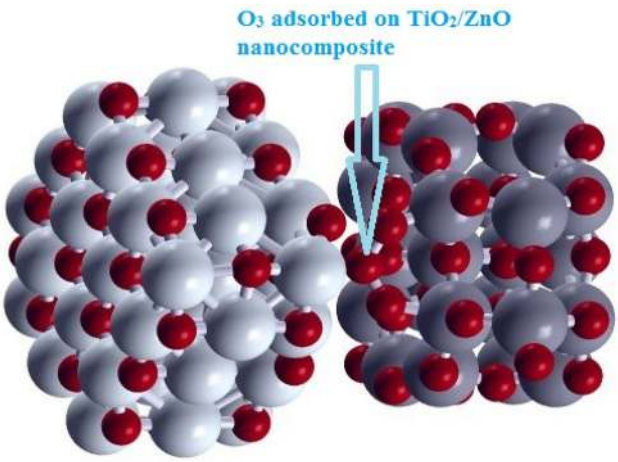

Keywords Interaction · Density functional theory · PDOS · NO_2 · O_3 · TiO_2/ZnO nanocomposite

Introduction

Titanium (Ti) and titanium alloys are some of the most important biomedical materials because of their biocompatibility, good mechanical properties, and outstanding corrosion resistance [1, 2]. It is well known that the surface of titanium atom possesses an excellent ability to be spontaneously oxidized into titanium oxide. This optimal

Electronic supplementary material The online version of this article (https://doi.org/10.1007/s40097-017-0244-3) contains supplementary material, which is available to authorized users.

✉ Amirali Abbasi
a_abbasi@azaruniv.edu

[1] Molecular Simulation Laboratory (MSL), Azarbaijan Shahid Madani University, Tabriz, Iran

[2] Computational Nanomaterials Research Group (CNRG), Azarbaijan Shahid Madani University, Tabriz, Iran

[3] Department of Chemistry, Faculty of Basic Sciences, Azarbaijan Shahid Madani University, Tabriz, Iran

surface property of TiO_2 is related to the excellent biocompatibility of the titanium atom [3]. Titanium dioxide (TiO_2) is one of the most favorable metal oxide semiconductors because of its excellent properties such as long-term stability, low cost and non-toxicity [4]. It has attracted great attention due to its versatile and tunable properties for applications in photo-catalysis [5], sensor devices [6], organic dye-sensitized solar cells [7], water splitting and air pollution control [8]. There are three important polymorphs of TiO_2, rutile, anatase, and brookite [9]. It possesses a wide band gap in the range of 3–3.2 eV, which prominently reduces its capability to be utilized in photocatalytic reactions. This wide band gap restricts the photosensitivity of TiO_2 to the ultraviolet (UV) region, decreasing the photocatalytic activity. Therefore, TiO_2 can only be employed in a minor area of the solar spectrum. Among different methods for improving the optical response of TiO_2, non-metal doping is the most broadly used method to increase the photocatalytic activity of TiO_2 [10, 11].

Recently, ZnO adsorbents have been extensively used as operative gas sensors for the detection and removal of harmful air pollutants. These semiconductor materials have been broadly studied owing to their outstanding physical and chemical stabilities, low cost, easy availability, and easy synthesis process [12]. ZnO nanostructures hold great potential as promising biocompatible materials for biomedical applications because of their advantages such as non-toxicity, biosafety, and their applicabilities in ZnO-based nanocarriers for drug delivery [13–18]. Over the past few years, several researchers have made great efforts to examine the particular properties of ZnO nanoparticles due to their biomedical applications, especially in cancer treatment [19]. Consequently, the unique optical and electronic properties of ZnO make it a favorable material to be utilized in various practical applications such as solar cells, gas sensor devices [20], piezoelectric transducers [21], photocatalysts, and photovoltaics [22]. ZnO nanomaterials can be simply synthesized at monitored chemical condition and small temperatures. Besides, some exceptional properties make ZnO as a suitable sensing material for gas sensing applications including novel structural arrangements, high single crystallinity surfaces and increased surface area to volume ratio [23–25]. Sensing gas molecules, specifically toxic air pollutants, is critical in environmental pollution reduction and agricultural and medical remediation [26]. Hence, sensitive solid-state sensors with low noise and low power consumption are extremely required. Peyghan et al. studied the adsorption behaviors and sensing properties of different nanoclusters and nanotubes of graphyne and carbon nitrides [27–29]. The main source of gas phase NO_2 molecule is motor vehicle exhausts and heavy industry. NO_2 is a major air pollutant, which has detrimental effects on the air quality with large contribution to the acid rain. NO_2 also causes by photochemical smog, which is harmful and irritant to human body, eyes, throat, nose and lungs [30]. On the other hand, O_3 molecule is a well-known air pollutant, which has detrimental impacts on respiratory tissues and ocular mucosa. The main target of tropospheric ozone in the human body is the lung, making harmful effects on the eyes and the nervous system [31]. The adsorption of different molecules on TiO_2-based nanoparticles and nanocomposites has been investigated in detail [32–39]. Due to the important role of NO_2 and O_3 emissions from the pollution control and toxicology point of view, harmful gas removal by efficient adsorbents would be increasingly demanded. Thus, it is of great significance to seek for novel sensors more fascinating than bare TiO_2 or ZnO such as multicomponent TiO_2/ZnO nanocomposites. Therefore, expanding the sensing materials from single component metal oxide semiconductor to multicomponent composite structure has become a challenging issue. Significantly, TiO_2-based two-component heterostructures, such as TiO_2/SnO_2 [40], TiO_2/ZnO [41, 42] and TiO_2/Fe_2O_3 [43] with enhanced sensing properties, have been efficiently constructed. TiO_2/ZnO heterostructures act as efficient candidates for improving sensing capabilities because they incorporate the physical and chemical properties of their individual components. Recently, TiO_2/ZnO nanocomposites have been synthesized successfully for various practical applications [44–48]. Figure 1 depicts a schematic representation of a metal oxide based gas sensor for toxic gas detection. In order to wholly exploit the possibilities of a TiO_2/ZnO composite material as effective gas sensor, a systematic theoretical study on the adsorption of gas molecules on a composite surface is conducted. In this

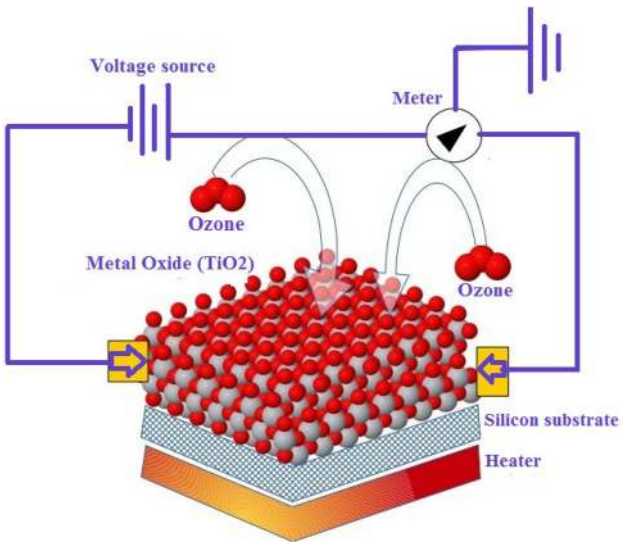

Fig. 1 Schematic representation of a metal oxide (TiO_2)-based gas sensor for O_3 detection

work, we have determined the most stable configuration for NO_2 and O_3 interaction with TiO_2/ZnO nanocomposites. Variations in the electronic structures of the adsorption systems induced by molecule adsorption are then examined. To the best of our knowledge, no prior theoretical study has been done on these subjects.

Method and computational details

Density functional theory [49, 50] calculations were carried out using the Open source Package for Material eXplorer (OpenMX3.8) code [51]. The techniques and systems used in OpenMX and their implementation are properly applied for the realization of large-scale ab initio electronic structure calculations on parallel computers. OpenMX conducts a systematic computation for the simulation of materials in nanoscale, leading to the systematic understanding of the interactions between complex materials based on the quantum mechanics. The basis sets in our calculations were chosen based on the linear combination of atomic orbitals, which were known as pseudo-atomic orbitals (PAOs). Converged results were obtained based on the energy cutoff of 150 Ry. The convergence threshold for energy and electronic structure computations was considered to be 10^{-4} Hartree/bohr. Exchange and correlation effects were incorporated within the generalized gradient approximation, using the Perdew–Burke–Ernzerhof (PBE) functional [52]. The van der Waals interactions were described using the Grimme's DFT-D2 methods [53]. Grimme and coworkers studied the effects of dispersion correction on the energetics and possible geometries of the complex systems [54–56]. The isosurfaces of the highest occupied and the lowest unoccupied molecular orbitals and the adsorption configurations were effectively visualized using the XCrysDen program [57]. It is well known that NO_2 molecule has a bent structure. The N–O bond length and corresponding O–N–O bond angle of NO_2 molecule have been estimated to be 1.20 Å and 134.3°, respectively. These achieved results are comparable with the previous gas phase data [58]. Also, O_3 molecule has a bent structure with calculated O–O bond length of 1.278 Å and O–O–O bond angle of 117°, based on GGA method, in line with previously reported theoretical and experimental values [59, 60].

The adsorption energies for the studied complexes were estimated using the following formula:

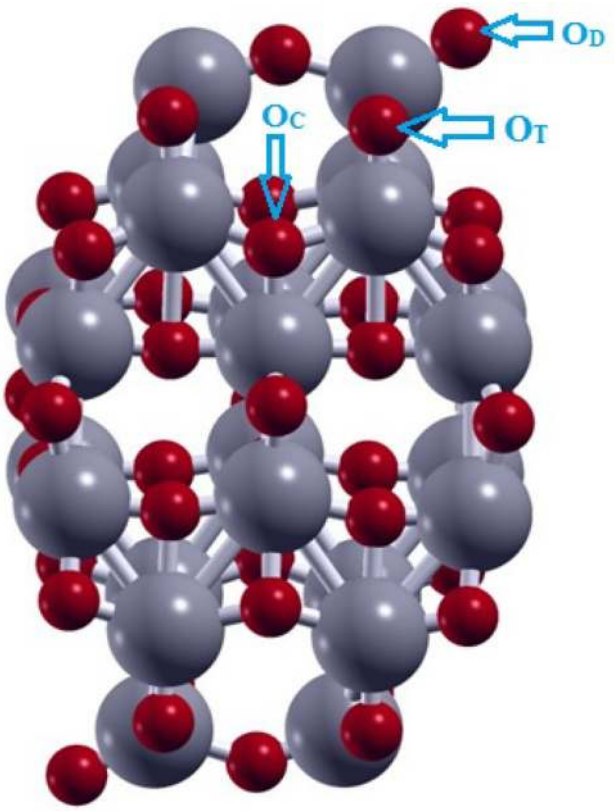

Fig. 2 Optimized structure of a pristine TiO_2 anatase nanoparticle: O_C, O_T and O_D denote threefold coordinated, twofold coordinated and dangling oxygen atoms, respectively. The gray and red balls denote titanium and oxygen atoms, respectively

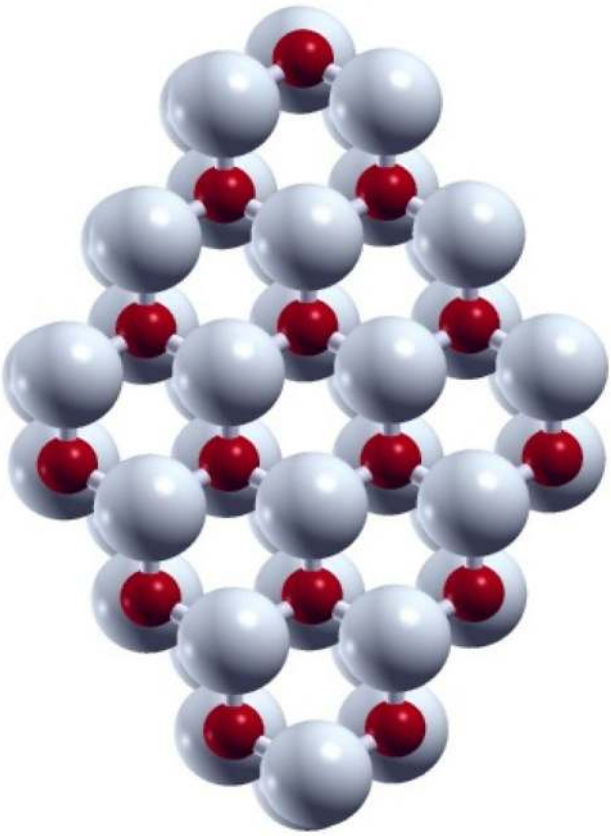

Fig. 3 Optimized structure of a pristine ZnO nanoparticle; the white and red balls represent zinc and oxygen atoms, respectively

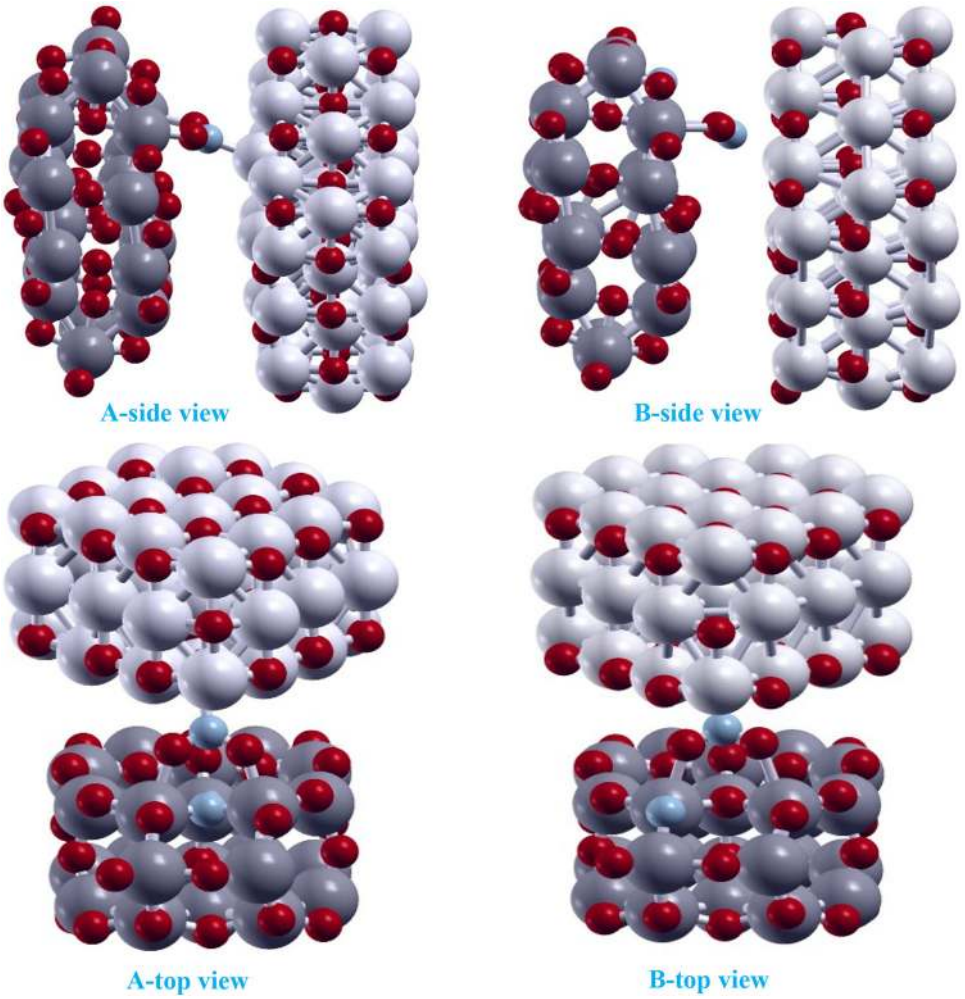

Fig. 4 Optimized geometry configurations of NO_2 molecule adsorbed on the N-doped TiO_2/ZnO nanocomposites. The fivefold coordinated titanium atoms were found to be the most stable binding sites on the TiO_2

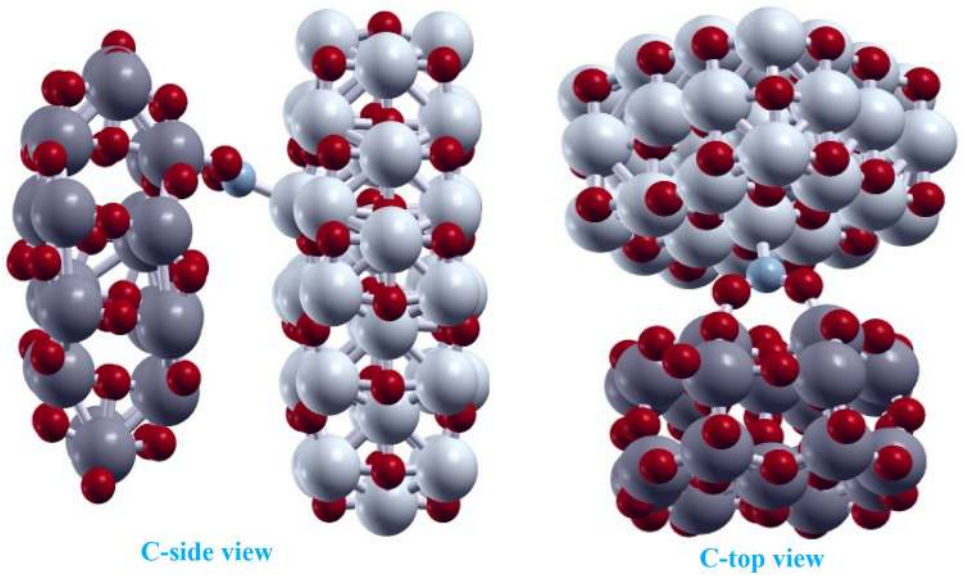

Fig. 5 Optimized geometry configurations of NO_2 molecule adsorbed on the undoped TiO_2/ZnO nanocomposites. The fivefold coordinated titanium and zinc atoms were found to be the most stable binding sites on the TiO_2

Table 1 Bond lengths (in Å) and angles (in degrees) for NO_2 molecule adsorbed on TiO_2/ZnO nanocomposites

Configuration	Newly formed Ti-O1 (Å)	Newly formed Ti-O2 (Å)	Zn-N (Å)	N-O1 (Å)	N-O2 (Å)	O–N–O angle (degree)
A	2.18	2.38	2.30	1.31	1.38	119.8
B	2.20	2.38		1.29	1.30	125.8
C	2.09	2.24	2.35	1.30	1.36	118.6
Non-adsorbed	–	–		1.20	1.20	134.3

$$E_{\text{ad}} = E_{(\text{composite} + \text{adsorbate})} - E_{\text{composite}} - E_{\text{adsorbate}}, \quad (1)$$

where $E_{(\text{composite} + \text{adsorbate})}$ corresponds to the total energy of combined composite with adsorbed molecule system, $E_{\text{composite}}$ and $E_{\text{adsorbate}}$ are the energies of the clean TiO_2/ZnO nanocomposite and free NO_2 or O_3 molecule, respectively. A negative adsorption energy represents that the adsorption process is strongly favored from the energy point of view. Thus, the obtained structures and final configurations are energy favorable.

TiO_2 anatase model: For TiO_2 anatase, the supercell approach was considered, which is based on the selection of an appropriate $3 \times 2 \times 1$ simulation supercell. We have chosen the unit cell using the American Mineralogists Database crystal structure database [61], which is an interface to a crystal structure database. This structure was developed by Wyckoff [62]. For our studied models, the nitrogen modified structures were obtained by introducing the nitrogen atoms into the oxygen vacancy of TiO_2, leading to the energy favorable N-doped TiO_2 nanoparticles. This substitution was performed at both O_C and O_T sites, representing the nitrogen doping at the middle of the particle (threefold coordinated oxygen site) and the twofold coordinated oxygen atom sites, respectively. The titanium atoms of the TiO_2 anatase were characterized as the fivefold coordinated and sixfold coordinated titanium sites, the former has more reactivity than the latter. It is also well known that the twofold coordinated oxygen can bind to the surface more efficiently, compared to the threefold coordinated atom [63]. Calculated cell parameters ($a = 3.784$ Å, $c = 9.621$ Å) are well consistent with experimental data ($a = 3.782$ Å, $c = 9.502$ Å) [64] and previous theoretical works [65, 66]. Figure 2 displays the optimized geometry of an undoped TiO_2 anatase nanoparticle constructed from the TiO_2 unit cell.

ZnO model: The unit cell of ZnO was also taken from "American Mineralogists Database" webpage reported by Kihara [67]. In the crystal structure of ZnO, we can see two types of oxygen atoms denoted by fourfold coordinated oxygen (4f-O) and threefold coordinated oxygen (3f-O) atoms. ZnO nanoparticle contains 90 atoms (45 Zn and 45 O atoms) without any dangling oxygen atoms. As a result, the atomic number ratio between Zn and O atoms is 1:1, and the total charge of the particle would be zero. The lattice parameters of wurtzite ZnO were calculated to be $a = b = 3.2502$ Å, $c = 5.205$ Å, which are in reasonable agreement with experimentally reported data [68]. The optimized structure of the considered ZnO nanocluster is shown in Fig. 3.

Results and discussion

NO_2 interacts with TiO_2/ZnO nanocomposites

The structure of TiO_2/ZnO nanocomposite was geometrically optimized. Similarly, both NO_2 and O_3 molecules were optimized initially. The modeling of the adsorption was achieved initially by placing NO_2 and O_3 molecules at the interface between TiO_2 and ZnO. Thus, at this interface, we can examine the adsorption of gas molecules on the nanocomposite. Optimized structures of the most stable NO_2 adsorptions on TiO_2/ZnO nanocomposites are presented in Figs. 4 and 5. The adsorption configurations of NO_2 on the considered nanocomposites were denoted by types A–C in these figures. The only difference between these structures is the final positioning of the NO_2 molecule with respect to the undoped or N-doped nanocomposite. Both oxygen atoms of the NO_2 move strongly towards the fivefold coordinated titanium atoms, bridging the fivefold coordinated titanium sites. In configuration A, NO_2 molecule adsorbs on the O_C-substituted nanocomposite. The

Table 2 Adsorption energies (in eV) for NO_2 and O_3 molecules adsorbed on the considered TiO_2/ZnO nanocomposites calculated from different methods and charge transfers between the TiO_2/ZnO nanocomposite and adsorbed molecule (|e|), calculated using Mulliken population analysis

Configuration	ΔE_{ads} (eV) PBE DFT-D2	Δq (e)
A	− 3.06 to 4.02	− 0.302
B	− 3.02 to 3.10	− 0.268
C	− 1.12 to 2.14	− 0.097
D	− 2.96 to 3.94	− 0.407
E	− 2.86 to 3.81	− 0.286
F	− 1.52 to 2.52	− 0.275

oxygen atoms were bonded to the titanium atoms and the nitrogen atom to the zinc site. Configuration B displays the adsorption of NO_2 on the O_T-substituted nanocomposite. It can be seen that there is no mutual interaction with the ZnO side of nanocomposite. Similar to configuration A, in configuration C, only the fivefold coordinated titanium atoms interact with the NO_2 molecule. Thus, NO_2 molecule reacts with the TiO_2 side of pristine TiO_2/ZnO nanocomposite. In adsorption types A and C, there is a triple contacting point between the nanocomposite and NO_2 molecule and the side oxygen atoms interact with the fivefold coordinated titanium atoms of TiO_2, while the nitrogen atom moves towards the zinc atom. Configuration B presents a double contacting point, formed from the interaction of the oxygen atoms of NO_2 with TiO_2 side of nanocomposite.

Table 1 summarizes the distance and angles parameters for the important bonds and angles of the NO_2 molecule before and after the adsorption process. When NO_2 molecule interacts with the nanocomposite, there was an elongation in the range of 0.11–0.16 Å for the bond lengths of N–O. The reason is that the electronic density increases at the middle of the newly formed bonds between the TiO_2/ZnO and NO_2 molecule. In other words, it was transferred from the N–O bonds to the newly formed Ti–O bonds between the nanocomposite and NO_2 molecule. This N–O bond elongation of NO_2 molecule makes that the N–O bonds to be weakened after the adsorption process. The bond angle of the optimized NO_2 molecule in gas phase is about 134.3°; after the adsorption, there is a decrease in O–N–O angle ranging from 10–15°. This decrease in the bond angle values is in reasonable consistency with the elongation of bond lengths. Table 2 summarizes the adsorption energies of NO_2 molecules on the considered TiO_2/ZnO nanocomposites. Clearly, the adsorption energies were increased from the undoped nanocomposite to the N-doped one. The results of this table indicate that the adsorption of NO_2 molecule on the N-doped TiO_2/ZnO nanocomposite gives rise to the more stable complexes than the adsorption on the pristine one. In view of this conclusion, the highest

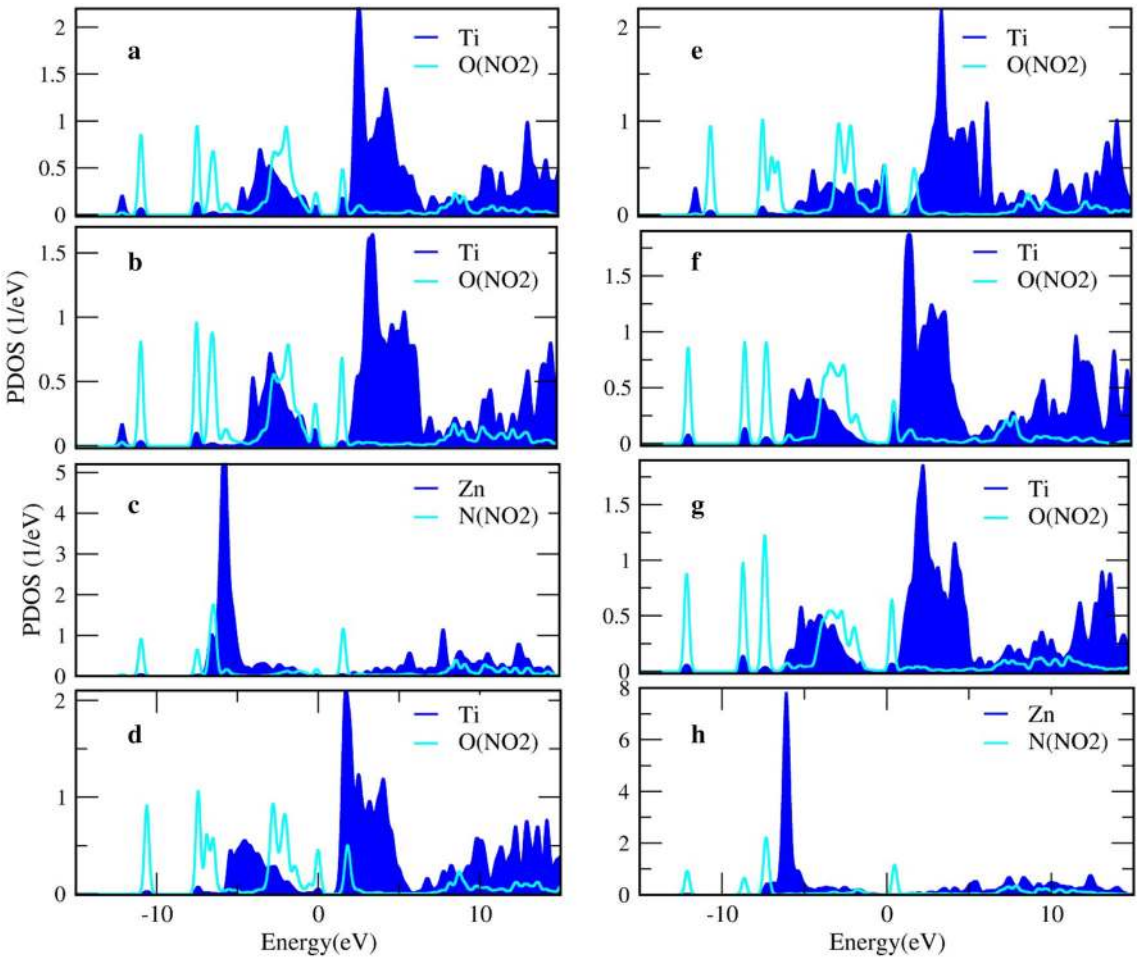

Fig. 6 PDOSs for the adsorption configurations of TiO_2/ZnO nanocomposites with adsorbed NO_2 molecules, **a–c** Configuration A; **d–e** Configuration B; **f–h** Configuration C

adsorption energy occurs in configuration A, whereas the lowest value belongs to configuration C. This is due to the fact that configuration A represents the interaction of NO_2 with N-doped nanocomposite. As can be seen, for configuration A, NO_2 molecule is oriented so that the oxygen atoms stand above the fivefold coordinated titanium site, and hence are able to form chemical bonds with the titanium atoms. The greater adsorption energy means stronger adsorption of NO_2 molecule to the surfaces. Thus, configuration A shows the strongest interaction of NO_2 molecule with the nanocomposite. The significant adsorption energy of configuration A also indicates that this configuration is the most stable binding site of NO_2 located on the nanocomposite.

Comparing the values, we found that the adsorption energy of configuration A is higher than that of configuration B, representing that the O_C-substituted nanocomposite strongly interacts with the NO_2 molecule. The effects of van der Waals interactions make that the adsorption energies to be enhanced after the adsorption. This increase was achieved by including the dispersion correction in the calculations. Gathering the results of adsorption energies, we found that the N-doped TiO_2/ZnO nanocomposite acts as a promising candidate to be utilized for the design of NO_2 sensor devices. To further examine the behavior of the NO_2 molecule on the TiO_2/ZnO nanocomposite, we have calculated the charge transfer values (see Table 2). The charge analysis based on Mulliken charges reveals a noticeable charge transfer from the NO_2 molecule to the nanocomposite. The highest charge transfer occurs in configuration A, while the lowest charge transfer belongs to configuration C. The results showed a direct relationship between the amount of charge transfer and the adsorption energies. Figure 6 shows the calculated projected density of states (PDOS) spectra for the adsorption configurations of TiO_2/ZnO nanocomposites with adsorbed NO_2 molecules. Panels (a–c) in this figure show the PDOSs of the titanium, oxygen and zinc atoms for configuration A, while panels (d–e) represent the PDOS spectra for configuration B. The significant overlaps

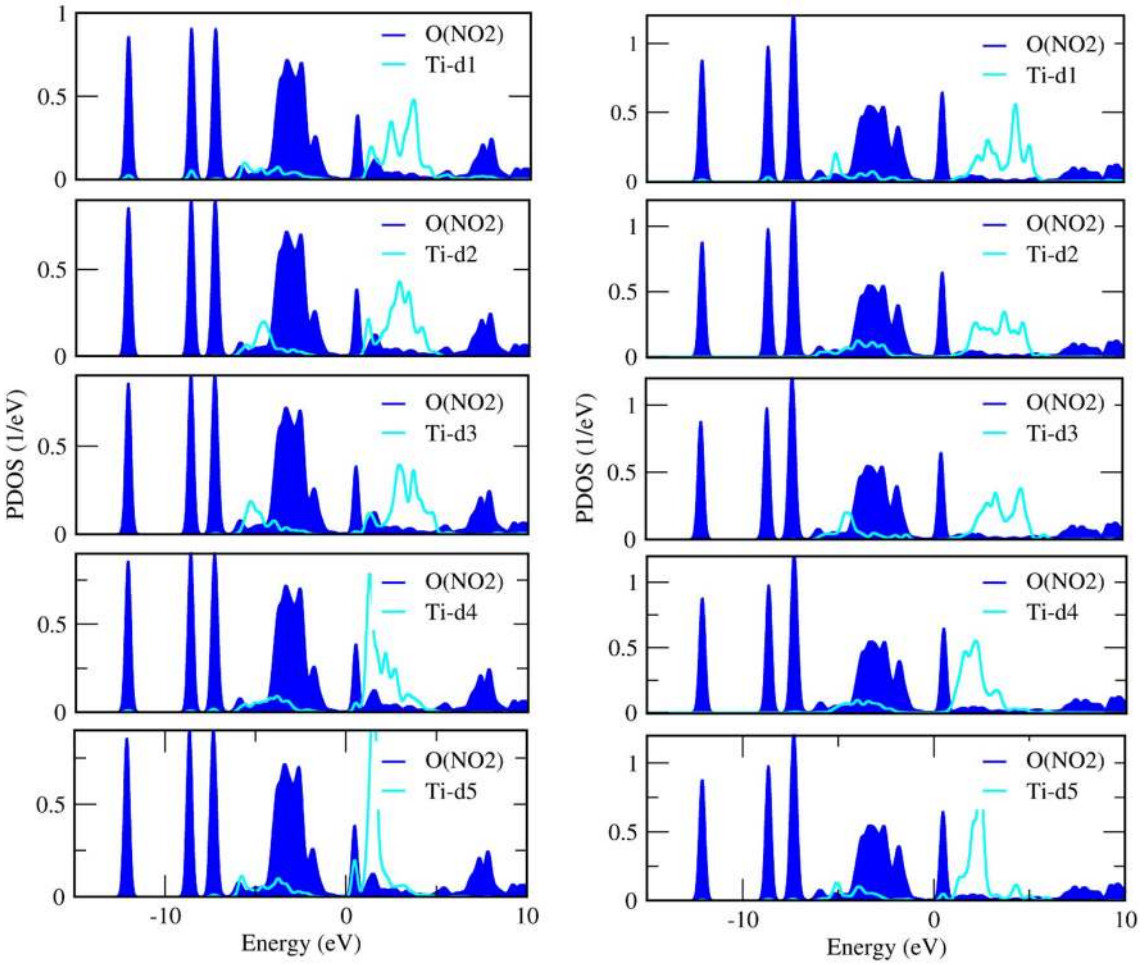

Fig. 7 PDOSs of the oxygen atom of NO_2 molecule, titanium atom and different d orbitals of the titanium atom for adsorption configurations of TiO_2/ZnO with adsorbed NO_2 molecule (configuration A)

between the PDOSs of the fivefold coordinated titanium atoms of TiO_2 and oxygen atoms of NO_2 indicate the formation of chemical Ti–O bonds between these two atoms. Also, from the PDOS overlaps of the nitrogen atom of NO_2 molecule and zinc atom, we found that there is strong interaction between them. Panels (d–e) show the PDOSs of the oxygen atoms of the NO_2 molecule and the titanium atoms, (configuration B), indicating noticeable overlaps between the PDOSs of the titanium and oxygen atoms. For configuration C with triple contacting point, the PDOS spectra of the titanium and oxygen atoms (panels (f–h)) exhibit considerable overlaps, representing the formation of chemical bonds between the interacting atoms. Figure 7 displays the PDOSs of the titanium, oxygen atoms of NO_2 molecule and different d orbitals of the titanium atom (configuration A). As can be seen from this figure, the PDOSs of the oxygen atom of NO_2 molecule and d^1 orbital of the titanium atom show large overlaps in some energy values. The isosurface plots of the highest occupied molecular orbitals (HOMOs) for NO_2 adsorbed TiO_2/ZnO nanocomposites are also illustrated in Fig. 8. As can be seen, the HOMOs of the adsorption systems show the accumulation of the electronic density over the adsorbed molecule.

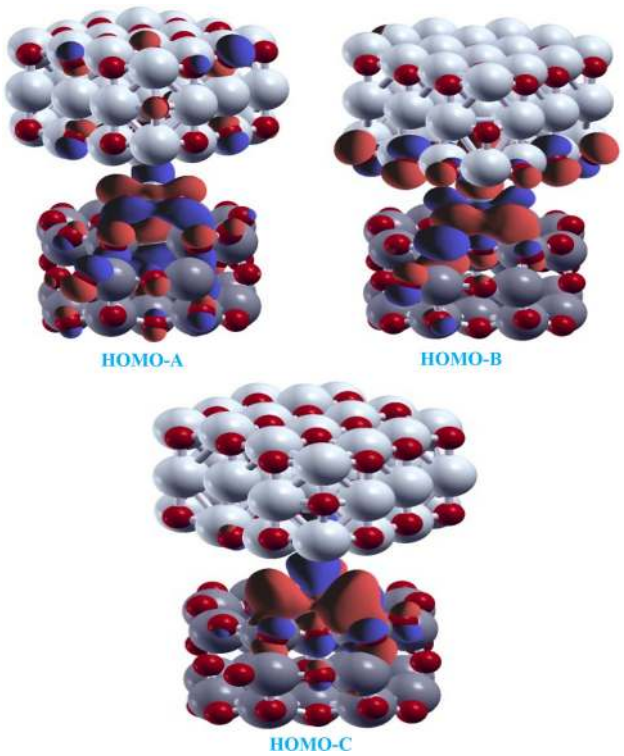

Fig. 8 Isosurfaces of the highest occupied molecular orbitals (HOMOs) for NO_2 adsorbed TiO_2/ZnO nanocomposites

O_3 interacts with TiO_2/ZnO nanocomposites

Figures 9 and 10 show the optimized geometry configurations of the N-doped and undoped TiO_2/ZnO nanocomposites with adsorbed O_3 molecules. The configurations of the interaction of O_3 molecule with TiO_2/ZnO nanocomposites were marked by adsorption types D–F. The only difference is the pattern of nitrogen doping into the oxygen vacancy of TiO_2, as well as the orientation of O_3 towards the nanocomposite. Configuration D represents the adsorption of O_3 on the O_C-substituted nanocomposite, while configuration E shows the favored orientation of O_3 over the O_T-substituted one. As can be seen from this figure, the undoped nanocomposite also interacts with O_3 molecule (configuration F). In all configurations, we can see that there is a double contacting point between the O_3 and TiO_2/ZnO nanocomposite, resulting from the coordination of the side oxygen atoms of the O_3 molecule to the fivefold coordinated titanium atoms. Interestingly, the central oxygen atom does not interact with the nanocomposite either from TiO_2 or ZnO side. Therefore, in the case of O_3 adsorption on the TiO_2/ZnO nanocomposites, the binding sites were located on the fivefold coordinated titanium atoms. Table 3 summarizes the bond lengths and bond angles for O_3 adsorption on the considered TiO_2/ZnO nanocomposites. The bond lengths of the O_3 undergo a noticeable change after the adsorption, the O–O bond lengths were stretched, and the elongation is in the range of 0.12–0.18 Å. This increase in the O–O bond length can be attributed to the transfer of electronic density from the O–O bonds of the O_3 to the newly formed Ti–O bonds between the TiO_2 side of nanocomposite and O_3 molecule. Similar to NO_2 adsorption, the O–O–O bond angles of the adsorbed O_3 were decreased in comparison with the gas phase O_3 molecule. Table 2 lists the calculated adsorption energies of the O_3 molecule on the considered nanocomposites. As can be seen from this table, the adsorption energies of N-doped nanocomposites (configurations D and E) are more negative than those of undoped ones (configuration F), indicating that the adsorption of O_3 molecule on the N-doped nanocomposite is more favorable in energy than that on the pristine one. The higher adsorption energy of N-doped nanocomposites with respect to the pristine ones indicates that the N-doped nanocomposites have higher sensing capability than the undoped ones. Thus, the most stable configuration corresponds to a bridge geometry of O_3 molecule towards the N-doped nanocomposite (configuration A), while the least stable one corresponds to configuration C. Therefore, the nitrogen doping strengthens the interaction between O_3 molecule and TiO_2/ZnO nanocomposite. To further examine the electronic properties of the gas–nanocomposite interaction, the projected density of states (PDOSs) were calculated for the most

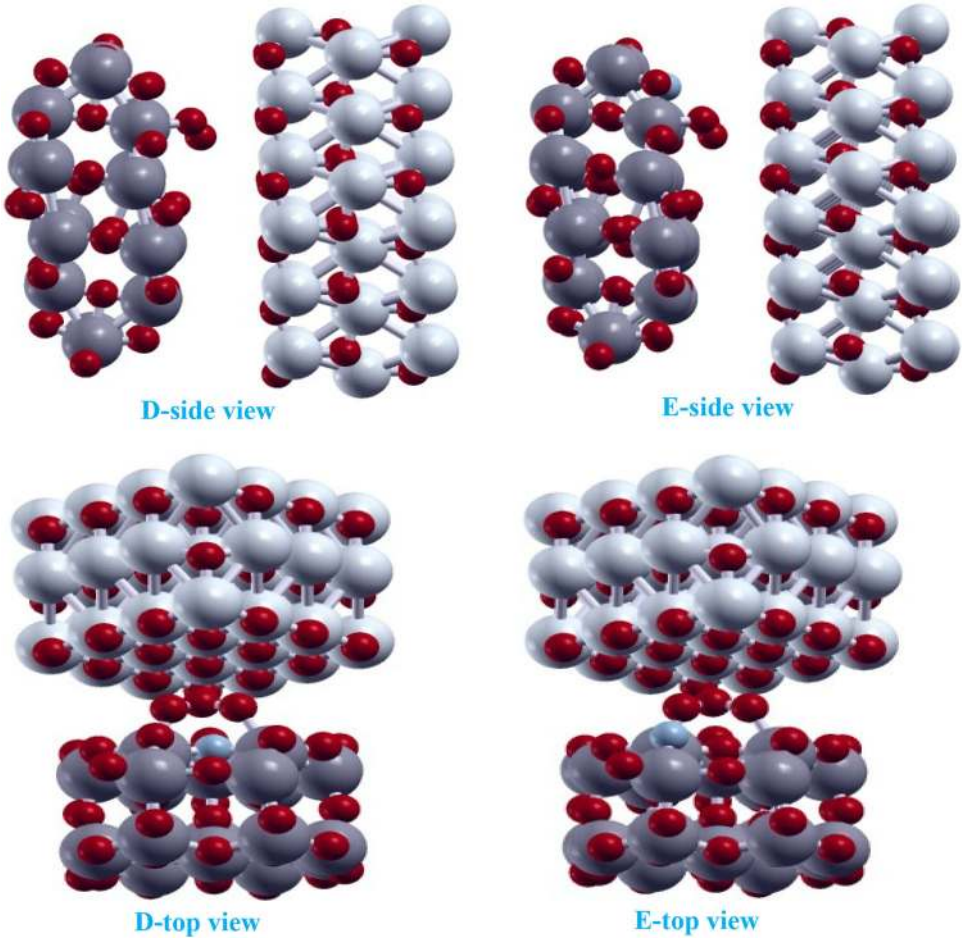

Fig. 9 Optimized geometry configurations of O_3 molecule adsorbed on the N-doped TiO_2/ZnO nanocomposites. The fivefold coordinated titanium atoms were found to be the most stable binding sites on the TiO_2

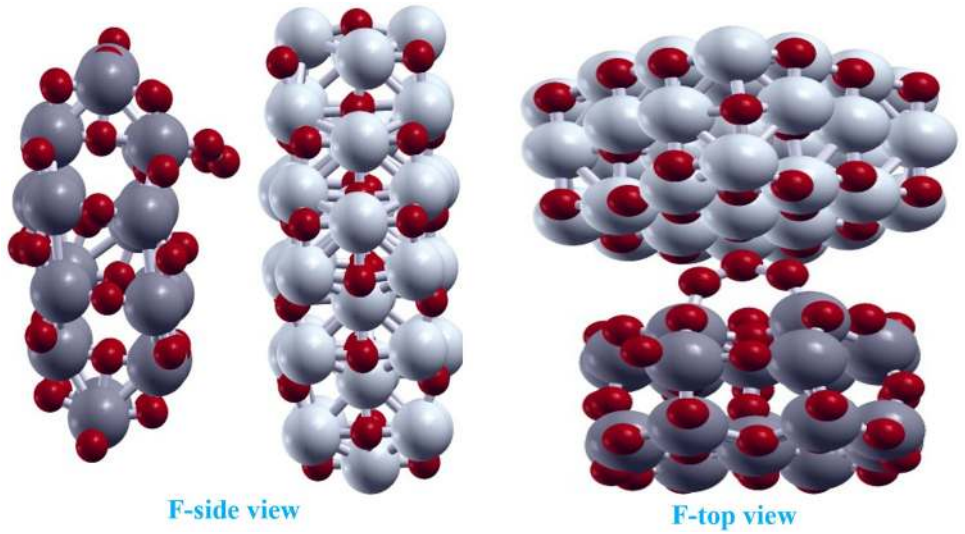

Fig. 10 Optimized geometry configurations of O_3 molecule adsorbed on the undoped TiO_2/ZnO nanocomposites. The fivefold coordinated titanium atoms were found to be the most stable binding sites on the TiO_2

stable structures of O_3 molecule adsorbed on the TiO_2/ZnO nanocomposites. Figure 11 displays the PDOSs of the fivefold coordinated titanium atoms and the side oxygen atoms of O_3 molecule (configurations D–F). As can be seen from this figure, there are significant overlaps between the PDOS spectra of the titanium and oxygen atoms. These overlaps confirm the formation of chemical Ti–O bonds between these atoms. Thus, O_3 molecule was chemisorbed on the TiO_2/ZnO nanocomposite. We have also calculated the PDOSs of the side oxygen atoms, titanium atom and

Table 3 Bond lengths (in Å) and angles (in degrees) for O_3 molecule adsorbed on TiO_2/ZnO nanocomposites

Configuration	Newly formed Ti-O1 (Å)	Newly formed Ti-O2 (Å)	O_C-O1 (Å)	O_C-O2 (Å)	O–O–O angle (degree)
D	2.05	2.19	1.40	1.45	118.7
E	2.06	2.20	1.42	1.46	120.2
F	1.97	2.15	1.40	1.55	121.2
Non-adsorbed	–	–	1.28	1.28	117.0

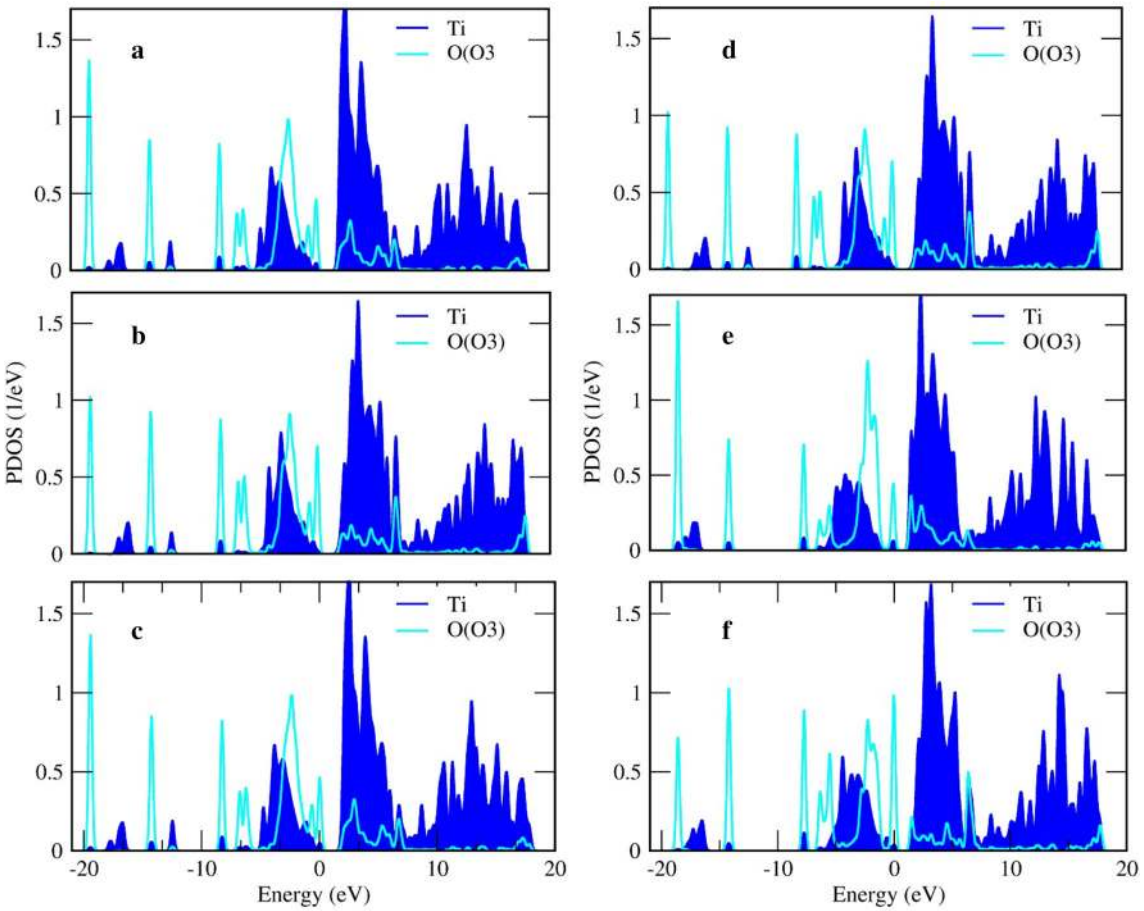

Fig. 11 PDOSs for the adsorption complexes of TiO_2/ZnO nanocomposites with adsorbed O_3 molecules, **a–b** Configuration D; **c–d** Configuration E; **e–f** Configuration F

different d orbitals of the titanium atom (see Fig. 12). In this case, the PDOS of d^1 orbital shows a greater overlap with the titanium atom compared with the other d orbitals. The isosurface plots of HOMOs for the adsorption O_3 molecule on the considered TiO_2/ZnO heterostructures are presented in Fig. 13. After the adsorption, the electronic densities in the HOMOs were largely concentrated over the O_3 molecule, which is in reasonable agreement with the transfer of electronic density from the O–O bonds of O_3 molecule to the newly formed bonds between the nanocomposite and O_3 molecule.

Vibrational frequencies

We have calculated the vibrational frequencies of free NO_2 molecule, and the gas molecules in a complex adsorption system. For brevity, we only reported the results for one configuration only (configuration A). The calculated vibrational frequencies are summarized in Table S1. The calculated vibrational frequencies for adsorbed NO_2 differ largely from the free NO_2 molecule, consistent with the strong adsorption of NO_2 to the TiO_2/ZnO nanocomposite. The results indicate that the symmetric and asymmetric

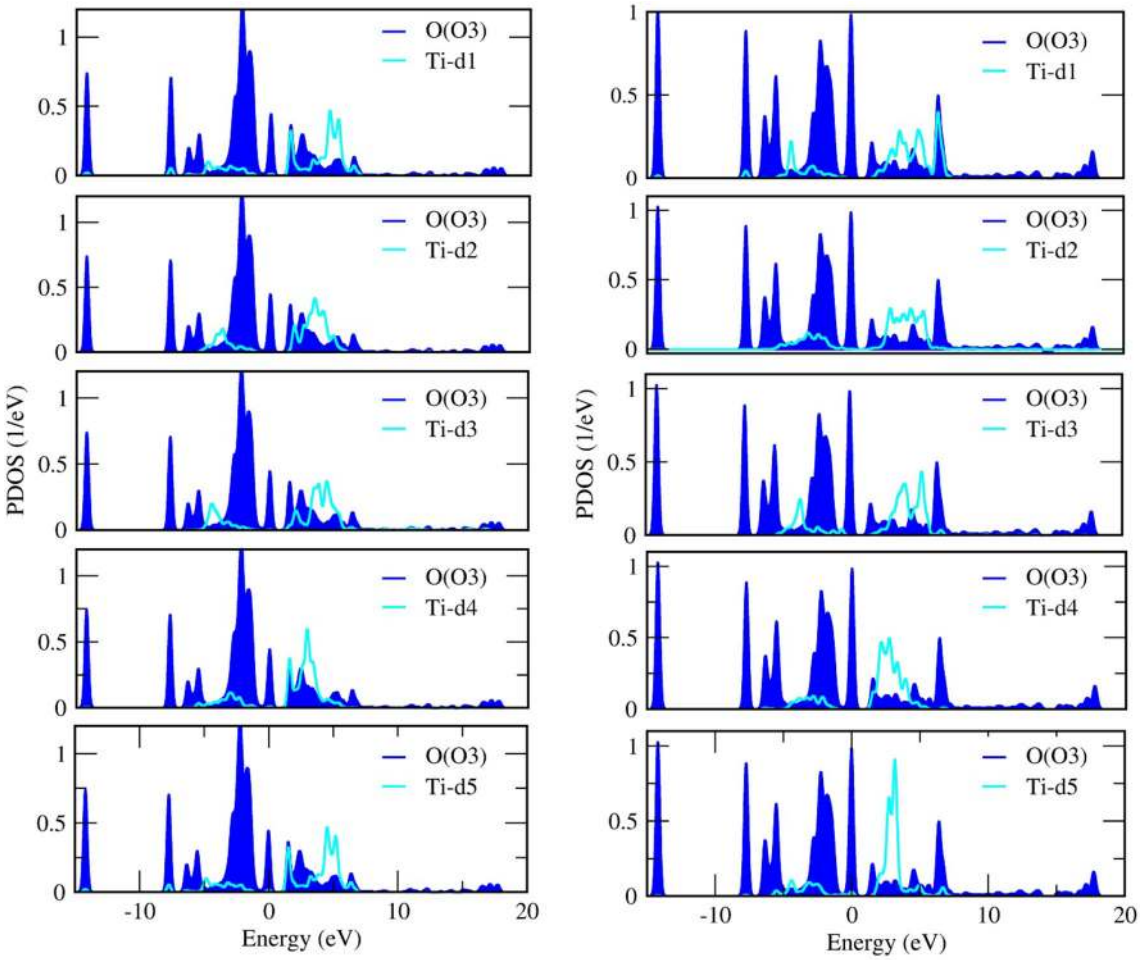

Fig. 12 PDOSs of the oxygen atom of O_3 molecule, titanium atom and different d orbitals of the titanium atom for adsorption configurations of TiO_2/ZnO with adsorbed NO_2 molecule (configuration D)

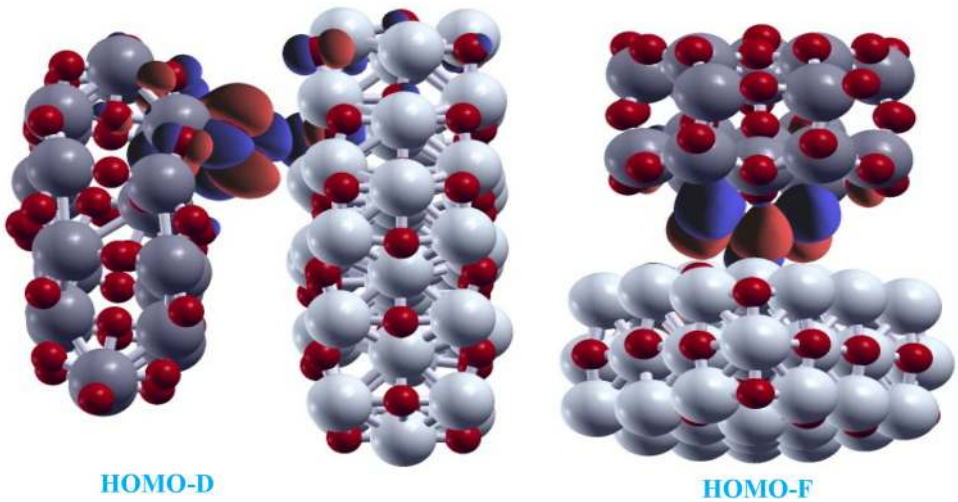

Fig. 13 Isosurfaces of the highest occupied molecular orbitals (HOMOs) for O_3 adsorbed TiO_2/ZnO nanocomposites

stretches were shifted to a lower frequency. The bending stretch mode was shifted to the higher frequency (blue-shift), indicating the highest shift for configuration A. However, the variations are relatively minor. In the case of configuration A, the shift in asymmetric stretch is more than that in symmetric stretch. Our obtained vibrational frequencies are very close to the experimentally reported data [69].

Conclusions

We have performed a theoretical study of NO_2 and O_3 molecules on the TiO_2/ZnO nanocomposites using density functional theory (DFT) calculations. These adsorptions are carried out on the pristine and N-doped nanocomposites. We found that both these molecules are chemisorbed on the nanocomposite surface, representing a bridge geometry of the gas molecule at the interface region. The results suggest that the gas sensing capability of TiO_2/ZnO is critically affected by nitrogen doping. The N-doped TiO_2/ZnO nanocomposites have higher sensing capability than the pristine ones. The results also suggest that gas molecules adsorption on the N-doped heterostructures leads to the more stable configurations than the adsorption on the undoped one, indicating that NO_2 and O_3 interaction with N-doped nanocomposite is strongly favored. For both cases, the least stable adsorption geometry corresponds to a bridge geometry of gas molecule on the pristine nanocomposite, whereas the most stable geometry belongs to N-doped configurations. After the adsorption, the N–O bonds of the NO_2 and the O–O bonds of the O_3 molecules were stretched. By taking van der Waals interactions into account, we found that the adsorption energies were increased. The charge analysis was performed based on the Mulliken population method, which indicates that the charge was transferred from the adsorbed molecules to the TiO_2/ZnO heterostructure. The large overlaps in the PDOS spectra of the interacting atoms represent the formation of chemical bonds between them. Consequently, the N-doped TiO_2/ZnO nanocomposite holds a great potential to be utilized in the design of NO_2 and O_3 sensor devices.

Acknowledgements This work has been supported by Azarbaijan Shahid Madani University.

Open Access This article is distributed under the terms of the Creative Commons Attribution 4.0 International License (http://creativecommons.org/licenses/by/4.0/), which permits unrestricted use, distribution, and reproduction in any medium, provided you give appropriate credit to the original author(s) and the source, provide a link to the Creative Commons license, and indicate if changes were made.

References

1. Liu, X.Y., Chub, P.K., Ding, C.: Surface modification of titanium, titanium alloys, and related materials for biomedical applications. Mater. Sci. Eng. R **47**, 49–121 (2004)
2. Lu, X., Leng, Y., Zhang, X., Xu, J., Qin, L., Chan, C.: Comparative study of osteoconduction on micromachined and alkali-treated titanium alloy surfaces in vitro and in vivo. Biomaterials **26**, 1793–1801 (2005)
3. Lu, X., Zhao, Z., Leng, Y.: Biomimetic calcium phosphate coatings on nitric acid treated titanium surfaces. Mater. Sci. Eng. C **27**, 700–708 (2007)
4. Shibata, Y., Irie, H., Ohmori, M., Nakajima, A., Watanabe, T., Hashimoto, K.: Comparison of photochemical properties of brookite and anatase TiO_2 films. Phys. Chem. Chem. Phys. **6**, 1359–1362 (2007)
5. Fernandez-Garcia, M., Martinez-Arias, A., Hanson, J.C., Rodriguez, J.A.: Nanostructured oxides in chemistry: characterization and properties. J. Chem. Rev. **104**, 4063–4104 (2004)
6. Zhang, Y., Zhang, C.R., Wang, W., Gong, J.J., Liu, Z.J., Chen, H.S.: Density functional theory study of a-cyanoacrylic acid adsorbed on rutile TiO_2 (1 1 0) surface. Comp. Theor. Chem. **1095**, 125–133 (2016)
7. Zhang, C.R., Han, L.H., Zhe, J.W., Jin, N.Z., Wang, D.B., Wang, X., Wu, Y.Z., Chen, Y.H., Liu, Z.J., Chen, H.S.: Tuning the electronic structures and related properties of Ruthenium-based dye sensitizers by ligands: a theoretical study and design. Comput. Theor. Chem. **1017**, 99–108 (2013)
8. Mendizabal, F., Lopéz, A., Arratia-Pérez, R., Zapata-Torres, G.: Interaction of LD14 and TiO_2 in dye-sensitized solar-cells (DSSC): a density functional theory study. Comput. Theor. Chem. **1070**, 117–125 (2015)
9. Li, X., Gao, H., Liu, G.: A LDA+U study of the hybrid graphene/anatase TiO_2 nanocomposites: interfacial properties and visible light response. Comput. Theor. Chem. **1025**, 30–34 (2013)
10. Nambu, A., Graciani, J., Rodriguez, J.A., Wu, Q., Fujita, E., Sanz, J.F.: N doping of TiO2 (110) Photoemission and density-functional studies. J. Chem. Phys. **125**(9), 094706 (2006)
11. Rumaiz, A.K., Woicik, J.C., Cockayne, E., Lin, H.Y., Jaffari, G.H., Shah, S.I.: Oxygen vacancies in N doped anatase TiO2: experiment and first-principles calculations. J Appl. Phys. Lett. **95**(26), 262111 (2009)
12. Wang, Z.L.: Zinc oxide nanostructures: growth, properties and applications. J. Phys.: Condens. Matter **16**, R829 (2004)
13. Nel, A., Xia, T., Madler, L., Li, N.: Toxic potential of materials at the nanolevel. Science **311**, 622–627 (2006)
14. Rakshit, S., Vasudevan, S.: Trap-state dynamics in visible-light-emitting ZnO:MgO nanocrystals. J. Phys. Chem. C **112**, 4531–4537 (2008)
15. Bohle, D.S., Spina, C.J.: The relationship of oxygen binding and peroxide sites and the fluorescent properties of zinc oxide semiconductor nanocrystals. J. Am. Chem. Soc. **129**, 12380–12381 (2007)
16. Xiong, H.M., Xu, Y., Ren, Q.J., Xia, Y.Y.: Stable aqueous ZnO@polymer core − shell nanoparticles with tunable photoluminescence and their application in cell imaging. J. Am. Chem. Soc. **130**, 7522–7523 (2008)
17. Wang, H., Wingett, D., Engelhard, M.H.: Fluorescent dye encapsulated ZnO particles with cell-specific toxicity for potential use in biomedical applications. J. Mater. Sci. **20**, 11–22 (2009)
18. Dhobale, S., Thite, T., Laware, S.L.: Zinc oxide nanoparticles as novel alpha-amylase inhibitors. J. Appl. Phys. **104**, 094907 (2008)
19. Hanley, C., Layne, J., Punnoose, A.: Preferential killing of cancer cells and activated human T cells using ZnO nanoparticles. Nanotechnology **19**, 295103–295113 (2008)
20. Spencer, M.J.S., Yarovsky, I.: ZnO Nanostructures for Gas Sensing: interaction of NO_2, NO, O, and N with the ZnO (1010) Surface. J. Phys. Chem. C **114**(24), 10881–10893 (2010)
21. Shi, J., Starr, M.B., Xiang, H., Hara, Y., Anderson, M.A., Seo, J.H., Ma, Z., Wang, X.: Interface engineering by piezoelectric potential in ZnO-based photoelectrochemical anode. Nano Lett. **11**, 5587 (2011)
22. Li, L., Zhai, T., Bando, Y., Golberg, D.: Recent progress of one-dimensional ZnO nanostructured solar cells. Nano Energy **1**(1), 91–106 (2012)

23. Catto, A.C., da Silva, L.F., Ribeiro, C., Bernardini, S., Aguir, K., Longo, E., Mastelaro, V.R.: An easy method of preparing ozone gas sensors based on ZnO nanorods. RSC Adv. **5**, 19528–19533 (2015)
24. Xu, H., Zhang, R.Q., Tong, S.Y.: Interaction of O_2, H_2O, N_2, and O_3 with stoichiometric and reduced ZnO (1010) surface. Phys. Rev. B **82**, 155326 (2010)
25. Kortidis, I., Moschovis, K., Mahmoud, F.A., Kiriakidis, G.: Structural analysis of aerosol spray pyrolysis ZnO films exhibiting ultra-low ozone detection limits at room temperature. Thin. Solid. Films **518**, 1208–1213 (2009)
26. Rai, P., Raj, S., Ko, K.J., Park, K.K., Yu, Y.T.: Synthesis of flower-like ZnO microstructures for gas sensor applications. Sens. Actuators. B **178**, 107–112 (2013)
27. Peyghan, A.A., Soleymanabadi, H.: Computational study on ammonia adsorption on the X12Y12 nanoclusters (X = B, Al and Y = N, P). Curr. Sci. **108**, 00113891 (2015)
28. Peyghan, A.A., Rastegar, S.F., Hadipour, N.L.: DFT study of NH_3 adsorption on pristine, Ni- and Si-doped graphynes. Phys. Letts. A. **378**, 2184–2190 (2014)
29. Beheshtian, J., Noei, M., Soleymanabadi, H., Peyghan, A.A.: Ammonia monitoring by carbon nitride nanotubes: a density functional study. Thin. Solid. Films **534**, 650–654 (2013)
30. Hesterberg, T.W., Bunn, W.B., McClellan, R.O., Hamade, A.K., Long, C.M., Valberg, P.A.: Crit. Rev. Toxicol. **39**, 743–781 (2009)
31. Felix, E.P., Filho, J.P., Garcia, G., Cardoso, A.A.: A new fluorescence method for determination of ozone in ambient air. Microchem. J. **99**(2), 530–534 (2011)
32. Abbasi, A., Sardroodi, J.J.: A first-principles study of the interaction of aspirin with nitrogen-doped TiO_2 anatase nanoparticles. Nanomed. Res. J. **1**(2), 69–78 (2016)
33. Abbasi, A., Sardroodi, J.J.: A theoretical study on the adsorption behaviors of Ammonia molecule on N-doped TiO2 anatase nanoparticles: applications to gas sensor devices. Int. J. Nano Dimens. **7**, 349–359 (2016)
34. Abbasi, A., Sardroodi, J.J.: Van der Waals corrected DFT study on the adsorption behaviors of TiO_2 anatase nanoparticles as potential molecule sensor for thiophene detection. J. Water Environ. Nanotechnol. **2**, 52–65 (2017)
35. Abbasi, A., Sardroodi, J.J., Ebrahimzadeh, A.R.: TiO_2/Gold nanocomposite as an extremely sensitive molecule sensor for NO_2 detection: a DFT study. J. Water Environ. Nanotechnol. **1**, 55–62 (2016)
36. Abbasi, A., Sardroodi, J.J.: A theoretical investigation of the interaction of Immucillin-A with N-doped TiO_2 anatase nanoparticles: applications to nanobiosensors and nanocarriers. Nanomed. Res. J. **1**(3), 128–138 (2017)
37. Zuas, O., Budiman, H., Hamim, N.: Anatase TiO_2 and mixed M-Anatase TiO_2 (M = CeO_2 or ZrO_2) nano powder: synthesis and characterization. Int. J. Nano Dimens. **4**(1), 7–12 (2013)
38. Otoufi, M.K., Shahtahmasebebi, N., Kompany, A., Goharshadi, E.: Systematic growth of Gold nanoseeds on silica for Silica@Gold core-shell nanoparticles and investigation of optical properties. Int. J. Nano Dimens. **5**, 525–531 (2014)
39. Habibpour, R., Kashi, E., Vaziri, R.: Computational study of electronic, spectroscopic and chemical properties of Cun(n = 2–8) nanoclusters for CO adsorption. Int. J. Nano Dimens. **8**(2), 114–123 (2017)
40. Chen, G., et al.: High-energy faceted SnO_2-coated TiO_2 nan-belt heterostructure for near-ambient temperature-responsive ethanol sensor. ACS Appl. Mater. Interfaces **7**, 24950–24956 (2015)
41. Park, S., et al.: Enhanced ethanol sensing properties of TiO_2/ZnO core-shell nanorod sensors. Appl. Phys. A **115**, 1223–1229 (2014)
42. Lou, Z., et al.: A class of hierarchical nanostructures: ZnO surface functionalized TiO_2 with enhanced sensing properties. RSC Adv. **3**, 3131–3136 (2013)
43. Zhu, C.L., et al.: Fe_2O_3/TiO_2 tube-like nanostructures: synthesis, structural transformation and the enhanced sensing properties. ACS Appl. Mater. Interfaces **4**, 665–671 (2012)
44. Karunakaran, C., Abiramasundari, G., Gomathisankar, P., Manikandan, G., Anandi, V.: Preparation and characterization of ZnO–TiO_2 nanocomposite for photocatalytic disinfection of bacteria and detoxification of cyanide under visible light. Mater. Res. Bull. **46**(10), 1586–1592 (2011)
45. Habib, M.A., Shahadat, M.T., Bahadur, N.M., Ismail, I.M.I., Mahmood, A.J.: Synthesis and characterization of ZnO-TiO_2 nanocomposites and their application as photocatalysts. Int. Nano Lett. **3**(5), 1–8 (2013)
46. Yadav, B.C., Srivastava, R., Dwivedi, C.D.: Synthesis and characterization of ZnO–TiO_2 nanocomposite and its application as a humidity sensor. Philos. Mag. **88**(8), 1113–1124 (2008)
47. Bansal, P., Bhullar, N., Sud, D.: Studies on photodegradation of malachite green using TiO_2/ZnO photocatalyst. Desalination Water Treat. **12**, 108–113 (2009)
48. Bansal, P., Bhullar, N., Sud, D.: Heterostructured TiO_2/ZnO–excellent nanophotocatalysts for degradation of organic contaminants in aqueous solution. Desalination Water Treat. **52**, 7004–7014 (2014)
49. Hohenberg, P., Kohn, W.: Inhomogeneous electron gas. J. Phys. Rev. **16**, B864–B868 (1964)
50. Kohn, W., Sham, L.: Self-consistent equations including exchange and correlation effects. J. Phys. Rev. **140**, A1133–A1138 (1965)
51. Ozaki, T., Kino, H., Yu, J., Han, M.J., Kobayashi, N., Ohfuti, M., Ishii, F., et al.: The code OpenMX, pseudoatomic basis functions, and pseudopotentials. http://www.openmxsquare.org (2017). Accessed 2 Mar 2017
52. Perdew, J.P., Burke, K., Ernzerhof, M.: Generalized gradient approximation made simple. J. Phys. Rev. Lett. **78**, 1396 (1981)
53. Grimme, S.: Semiempirical GGA-type density functional constructed with a long-range dispersion correction. J. Comput. Chem. **27**, 1787–1799 (2006)
54. Piane, M.D., Corno, M., Ugliengo, P.: Does dispersion dominate over h-bonds in drug-surface interactions? the case of silica-based materials as excipients and drug-delivery agents. J. Chem. Theory Comput. **9**(5), 2404–2415 (2013)
55. Piane, M.D., Vaccari, S., Corno, M., Ugliengo, P.: Silica-based materials as drug adsorbents: first principle investigation on the role of water microsolvation on ibuprofen adsorption. Phys. Chem. A. **118**(31), 5801–5807 (2014)
56. Tasinato, N., Moro, D., Stoppa, P., Pietropolli, C.A., Toninello, P., Giorgianni, S.: Adsorption of F_2Cdbnd CFCl on TiO_2 nanopowder: structures, energetics and vibrational properties from DRIFT spectroscopy and periodic quantum chemical calculations. Appl. Surf. Sci. **353**, 986–994 (2015)
57. Koklj, A.: Computer graphics and graphical user interfaces as tools in simulations of matter at the atomic scale. J. Comput. Mater. Sci. **28**, 155–168 (2003)
58. Breedon, M., Spencer, M., Yarovsky, I.: Adsorption of NO2 on oxygen deficient ZnO (2110) for gas sensing applications: a DFT study. J. Phys. Chem. C **114**(39), 16603–16610 (2010)
59. Trambarulo, R., Gosh, S.N., Burrus, C.A., Gordy, J.W.: The molecular structure, dipole moment, and g factor of ozone from its microwave spectrum. J. Chem. Phys. **21**, 851 (1953)
60. Katrib, Y., Martin, S.T., Hung, H.M., Rudich, Y., Zhang, H., Slowik, J.G.: Products and mechanisms of ozone reactions with oleic acid for aerosol particles having core-shell morphologies. J. Phys. Chem. A **108**(32), 6686–6695 (2004)
61. The data available at http://rruff.geo.arizona.edu/AMS/amcsd.php
62. Wyckoff, R.W.G.: Crystal Structures, 2nd edn. Interscience Publishers, New York (1963)

63. Liu, J., Dong, L., Guo, W., Liang, T., Lai, W.: CO adsorption and oxidation on N-doped TiO_2 nanoparticles. J. Phys. Chem. C **117**, 13037–13044 (2013)
64. Burdett, J.K., Hughbanks, T., Miller, G.J., Richardson, J.W., Smith, J.V.: Structural-electronic relationships in inorganic solids: powder neutron diffraction studies of the rutile and anatase polymorphs of titanium dioxide at 15 and 295 K. J. Am. Chem. Soc. **109**, 3639–3646 (1987)
65. Spreafico, C., Vondele, J.V.: The nature of excess electrons in anatase and rutile from hybrid DFT and RPA. Phys. Chem. Chem. Phys. **16**, 26144–26152 (2014)
66. Lazzeri, M., Vittadini, A., Selloni, A.: Structure and energetics of stoichiometric TiO2 anatase surfaces. Phys. Rev. B. **65**, 119901 (2002)
67. Kihara, K., Donnay, G.: Anharmonic thermal vibrations in ZnO Model: 3-c, at T = 473 K. Can. Miner. **23**, 647–654 (1985)
68. Spencer, M.J.S.: Gas sensing applications of 1D-nanostructured zinc oxide: insights from density functional theory calculations. Prog. Mater Sci. **57**, 437–486 (2012)
69. CRC Handbook of Chemistry and Physics, Internet Version 2006; Lide, D.R. (ed.). Taylor and Francis, Boca Raton, FL (2006). Accessed 23 Jan 2008

Publisher's Note

Springer Nature remains neutral with regard to jurisdictional claims in published maps and institutional affiliations